Friction between two weakly adhering boundary lubricated surfaces in water

C. Drummond,[1,2] J. Israelachvili,[2] and P. Richetti[1,2]
[1]*Centre de Recherche Paul Pascal, CNRS-Université de Bordeaux 1, Avenue Schweitzer, 33600 Pessac Cedex, France*
[2]*Department of Chemical Engineering, University of California, Santa Barbara, California 93106, USA*
(Received 4 November 2002; published 20 June 2003)

The sliding of adhesive surfactant-bearing surfaces was studied with a surface forces apparatus nanotribometer. When the surfaces are fully immersed in an aqueous solution, the dynamic behavior is drastically different and more varied than under dry conditions. In solution, the shear stress exhibits at least five different velocity regimes. In particular, the sliding may proceed by an ''inverted'' stick-slip over a large range of driving velocities, this regime being bounded by smooth (kinetic) sliding at both lower and higher driving velocities. The general behavior of the system was studied in detail, i.e., over a large range of experimental conditions, and theoretically accounted for in terms of a general model based on the kinetics of formation and rupture of adhesive links (bonds) between the two shearing surfaces with an additional viscous term.

DOI: 10.1103/PhysRevE.67.066110 PACS number(s): 81.40.Pq, 46.55.+d

I. INTRODUCTION

Very often the friction between two surfaces sliding past each other exhibits a stick-slip motion even when the driving force or velocity is kept constant [1,2]. The stick-slip can be erratic, with stochastic spikes, or highly periodic, showing regular sawtooth oscillations. Several causes have been identified to be at the origin of such unsteady sliding [3]. First, rough or corrugated surfaces have long been known to produce irregular or regular stick-slip [1]. In a very general fashion, regular stick slip always arises when the interfacial friction decreases with the driving velocity *V and* the stiffness or compliance of the system is below some critical value [1–6]. This often arises with dry and boundary-lubricated surfaces and has been conceptualized in a number of phenomenological ''rate-and-state''models [2,7,8]. More recently, a ''phase-transition model'' has been proposed for the stick-slip observed in molecularly thin liquid films confined between smooth surfaces [9–11]. According to this model, during each stick-slip cycle, the film undergoes a transition between a static solidlike state (stick) and a kinetic liquidlike state (slip).

For all of these systems, the stick-slip oscillations occur between a high friction static state and a low friction kinetic state, and the transition from stick-slip to smooth sliding is observed to occur *above* some critical driving velocity V_c. An example of this type of transition, observed in the majority of tribological systems, is shown in Fig. 1(a). This friction trace as well as all the other ones presented hereinafter were measured between boundary lubricated surfaces with a tribometer version of the surface forces apparatus (SFA) [12], the surfaces being coated by self-assembled surfactant layers. For the results presented in Fig. 1(a), the coating consisted of a single monolayer of cethyl-trimethyl ammonium chloride (CTAC) on each surface and the measurements were performed under dry conditions. Similar friction traces have been previously obtained with other surfactants exposed to a vapor atmosphere under similar conditions as well as under controlled humidity [13].

In two recent papers [14,15], we have reported what appears to be a different class of behavior when the friction measurements are performed with the surfaces fully immersed in bulk aqueous surfactant solutions. An example is given in Fig. 1(b). The surfaces were now immersed in CTAC solution from which the surfactant was directly adsorbed. A stick-slip behavior with regular oscillations still occurs, but many trends of this unsteady regime are reversed with respect to the ones of the common stick-slip, which is why we called it ''inverted stick-slip'' [14]. One of these differences is that the unsteady regime now occurs *after* a smooth-sliding regime, which is observed at low velocities. In further contrast to the common scenario, the spikes of the

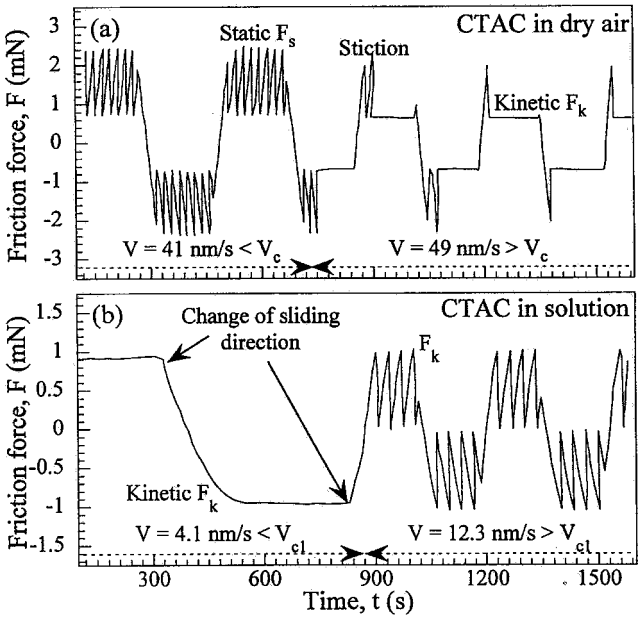

FIG. 1. Stick-slip–to–smooth-sliding transition. (a) Conventional stick-slip: In the stick-slip regime, at $V<V_c$, the friction force oscillates between the kinetic value F_k and a higher ''static'' value F_s. Above the critical driving velocity V_c, smooth sliding is observed. (b) Inverted stick-slip. The smooth-sliding regime is now observed at low velocities, $V<V_{c1}$. In the stick-slip regime, the friction force oscillates between the kinetic value F_k and a *lower* value F_{sk}. Note that after a change in the driving direction, no stiction spike is observed in the smooth-sliding regime at low velocities.

stick-slip oscillations are inverted, falling below the smooth kinetic baseline F_k, observed at lower velocity, instead of rising above it towards the static value F_s, as in Fig. 1(a). In fact, no indication of static friction is observed in this case even when the sliding starts from rest, regardless of the stopping time, or when the sliding direction is reversed in the smooth-sliding regime. In the common scenario [cf. Fig. 1(a)], a reversal of the sliding direction usually yields a stiction spike that precedes the smooth sliding. The low-frequency cycles in the friction traces in Fig. 1 are due to such direction reversals. No stiction peaks are observed in the case of the inverted stick-slip scenario, as can be observed in Fig. 1(b).

In this paper, we report the data we have cumulated on this unusual behavior. Most of it can be accounted for in terms of a general model based on the kinetics of formation and rupture of adhesive links between two shearing surfaces. The paper is organized as follows. In Sec. II, we describe the materials and the experimental technique used in this work. Section III is devoted to the experimental results. The generic profiles of the stress-velocity sliding curves in the different regimes are given in detail in this section. We review their dependence on the normal load, the temperature, and the bulk surfactant concentration. In Sec. IV, we present an adhesive friction model initially proposed by Schallamach 40 years ago [16], to which some modifications are added to improve the interpretation of the experimental curve. The discussion of the results in terms of the theoretical model is presented in Sec. V. Finally, the main conclusions of this study are presented in Sec. VI.

II. EXPERIMENT

A. Apparatus

All data reported in this paper have been obtained with a nanotribometer, a dynamic version of the (SFA), specially designed to investigate at the nanometer level the shear forces between two surfaces sliding past each other [12,17]. The surfaces are molecularly smooth mica sheets glued onto cylindrical lenses of radius $R \approx 2$ cm, using a thermosetting epoxy (EPIKON 1004, Shell Chemical Co.), which are mounted in the apparatus in a crossed configuration. This geometry, combined with the molecular smoothness of the mica surfaces, ensures a single contact point when the surfaces made to approach towards each other. The two surfaces can be approached (loading) or separated (unloading) with a distance accuracy of a few angstroms. An interferometric technique (FECO) is used to measure the separation between the surfaces D (to ± 2 Å), their local radii of curvature R around the contact position (to ± 0.1 mm), and when deformed under a normal load L, their elastically flattened area of contact, $A = \pi r^2$ (to ± 10 μm^2). A lateral relative motion of the surfaces is induced with voltage-driven piezoelectric bimorph strips supporting the lower surface [17]. Applying a triangular voltage signal to the bimorphs displaces this surface at a constant sliding velocity V. The surface is moved linearly in one direction until the maximum voltage is reached, and then the direction is reversed. The sliding amplitude ranges from a few nanometers to 25 μm, while the frequency can be varied between 10^{-3} and 10 Hz. The friction force F is measured with semiconductor strain gauges attached to a double-cantilever spring of stiffness K_m between 3000 and 9500 N/m, supporting the second (upper) surface. The resonance frequency of the mass-spring system was between 300 and 400 Hz. The temperature was controlled between 16 and 32 °C with an accuracy of better than 0.05 °C.

B. Materials and procedure

Four water-soluble surfactants with positively charged quaternary ammonium head groups were investigated, referred to in the text as CTAC, DDAB, gemini, and trimeric. CTAC has been purchased from Kodak with a higher quality grade and used as received. DDAB (didodecyldimethylammonium bromide), 12-2-12 gemini [ethanediyl-1,2-bis(dimethyldodecylammonium bromide)] [18], and 12-3-12-3-12 trimeric (methyldodecylbis[3-(dimethyldodecylammonio)propyl]ammonium tribromide) [18] were original. Gemini and trimeric surfactants are quaternary ammonium bromide oligomers, with dodecyl ammonium moieties connected at the ammonium group by ethyl or propyl chains [18]. All these cationic surfactants spontaneously adsorb on the negatively charged mica surfaces from aqueous solutions. For surfactant concentrations above the critical micelle concentration (CMC), the adsorbed films show a different morphology depending on the surfactant. A number of them adsorbed as flat bilayers, while the others formed rather modulated layers, suggesting the adsorption of globular or cylindrical micelles [19–22]. Adsorption on the mica surfaces was initiated in the SFA chamber by having the mica surfaces immersed in the surfactant solutions at a given concentration. After overnight adsorption, the coated surfaces, still immersed in the surfactant solution, were brought into contact. The friction measurements were performed under different normal loads, including loads large enough to induce the rupture of the adsorbed films. The normal force profile (force vs separation distance) between the coated surfaces was systematically measured before any friction study to determine the quality of the contact and the point of zero load.

III. RESULTS

Figure 2(a) shows a typical force profile measured between two cationic surfactant-coated mica surfaces in an aqueous solution [23]. In this example, we used the trimeric surfactant at a concentration of 8 CMC. At large separations, the expected long-range DLVO force due to the interaction of the charged adsorbed films is observed. Closer in, when the bilayers are only separated for a few angstroms, a hydration force barrier deviated the measured force profile from the predictions of the DLVO theory [23,24]. Along this steep branch, we were unable to detect any significant friction force, regardless of the sliding velocity and the morphology of the adsorbed films. At the largest loads that could be applied before the adsorbed films ruptured, the friction force was at the lower limit of the sensitivity of the device (~ 20 μN) with a corresponding weak signal emerging from the

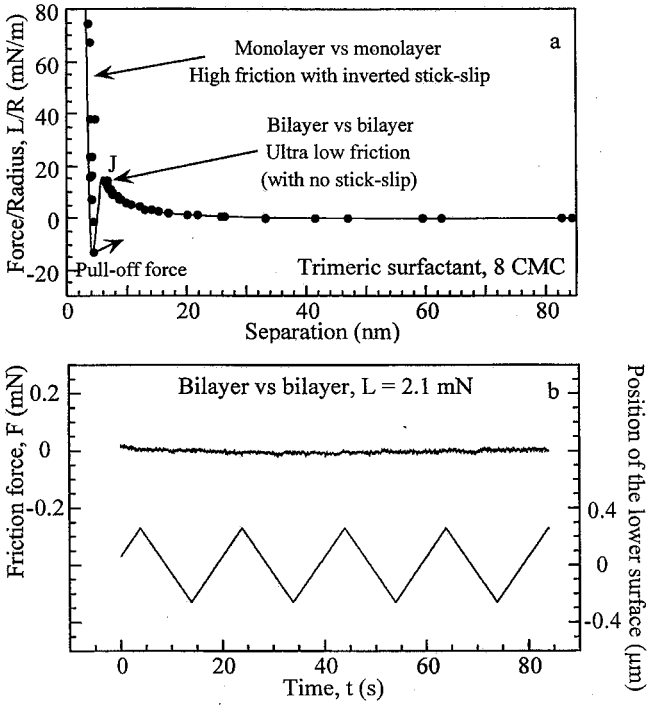

FIG. 2. (a) Normal force profile between two adsorbed trimeric bilayers in aqueous surfactant solution. Before the hemifusion, $D > 7$ nm, the friction between the bilayers is smooth and weak. In the hemifused state, the friction between the two contacting monolayers is large and may exhibit an inverted stick-slip. (b) Actual friction trace measured between two bilayers of the trimeric surfactant at $T = 26\,^{\circ}\mathrm{C}$ with a driving velocity $V = 0.05\ \mu$m/sec and a normal load $L = 2.1$ mN. The triangular signal is the actual position of the lower surface. The measurement evidences ultralow friction between the bilayer-covered surfaces.

noise. Such a friction trace is presented in Fig. 2(b). It has been measured between two trimer bilayers separated by 7 nm, i.e., almost at physical contact. The corresponding coefficient of friction, $\mu = F/L$ would be equal or less than 0.004, an extremely low value (as a reference, the kinetic friction coefficient of ice is around 0.03). This low friction without stick-slip may be related to what has been recently reported by Ravi *et al.* in study of aqueous salt solutions [25].

At larger loads, above the rupture threshold, we have observed two different behaviors depending upon the morphology of the adsorbed films. When the surfactant molecules adsorbed as cylindrical or globular micelles, the adsorbed films are almost completely expelled from the contact zone (interfacial rupture). However, it seems that a few isolated molecules or small patches remain trapped between the mica surfaces: the surface separation after this type of rupture was never zero, but varied between 0 and 5 Å.

On the other hand, when the surfactant molecules adsorb as flat bilayers, large loads trigger the hemifusion of the two bilayers into one bilayer [26], i.e., only the outer monolayer of each adsorbed bilayer is expelled from the contact zone (cohesive rupture). Hemifusion [Fig. 2(a)] brings the two adsorbed monolayers into an adhesive (hydrophobic) contact. The mica surfaces are then about 30 Å apart, depending on

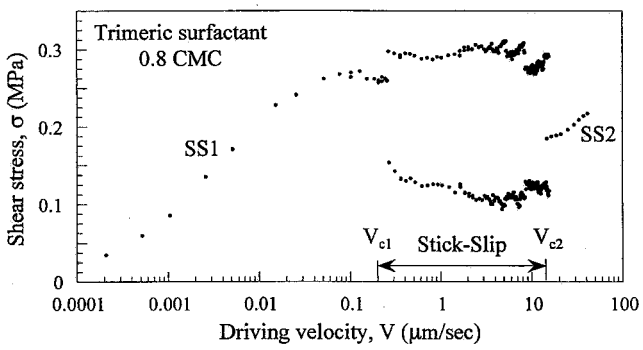

FIG. 3. Driving-velocity dependence of the spring force measured, while shearing two adsorbed monolayers of the 12-3-12-3-12 surfactant under a load of $L = 4.51$ mN at $T = 20\,^{\circ}\mathrm{C}$. The surfactant concentration in the bulk solution is 0.8 CMC. The smooth-sliding (SS1)–to–stick-slip transition occurs at $V_{c1} \approx 0.3\ \mu$m/s. Prior to the transition, the kinetic stress σ_k levels off at V_1 after a logarithmic σ-V dependence (shear-thinning regime). The quasi-smooth regime persists up to the transition at V_{c1}. At high driving velocities, a new transition to a smooth-sliding regime (SS2) is observed between 14 and 17 μm/s.

the surfactant. The hemifused state is clearly recognizable on the corresponding force profiles, being characterized by an almost vertical force barrier (hard wall) after a jump-in from point *J*, as illustrated in Fig. 2(a). After the jump, the two surfaces adhere in the central contact region but repel outside it, where the bilayers are preserved. A circular defect line or dislocationlike loop separates the two domains.

Once in the hemifused state, the friction forces become significant, in contrast to what is observed when the surfaces are still covered by complete bilayers under the same load. The inverted stick-slip scenario is observed when the surfaces are in this hemifused state. The measured friction traces are highly ''reversible'' and ''reproducible,'' in the sense that they do not change with time or sliding direction, and are identical under loading and unloading conditions. This is true both in the inverted stick-slip and smooth-sliding states.

The inverted stick-slip scenario was always found with the three surfactants we tested that have the ability to generate an adhesive monolayer-monolayer contact, namely, CTAC, 12-2-12 [18] and 12-3-12-3-12 surfactants [18]. We found it more convenient to work with the trimeric surfactant and most of the results presented in this paper have been obtained with this noncommercial surfactant [18]. To fully characterize the inverted stick-slip scenario, we pursued a thorough exploration of the relevant experimental parameters; in the next few sections, the response of the system to changes on sliding velocity, normal load, temperature, and bulk surfactant concentration are described in detail.

A. Driving velocity dependence

Figure 3 shows the typical variation of the shear stress $\sigma = F/A$ with driving velocity V at a fixed temperature and load when the mica surfaces are coated with the trimeric surfactant and brought together in the adhesive hemifused

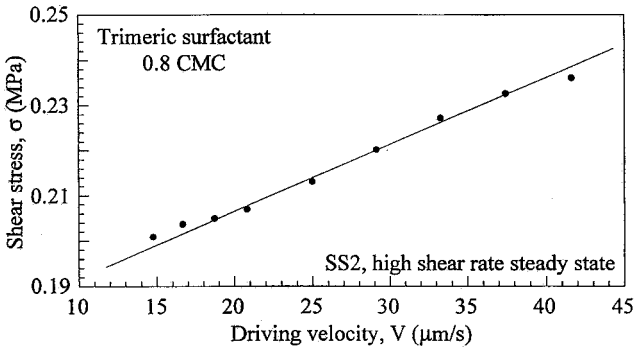

FIG. 4. Velocity dependence of the shear stress between two adsorbed monolayers of the trimeric 12-3-12-3-12 surfactant in the high velocity smooth-sliding regime. $L=4.51$ mN, $T=20\,^{\circ}$C.

state (monolayer-monolayer contact). The sliding σ-V curve presents at least four different regimes with an inverted stick-slip regime bounded by two steady smooth-sliding regimes. The smooth friction-velocity curves at low driving velocities increase roughly logarithmically with V, with no indication of a static friction. The absence of a yield stress and the increase of the friction force with driving speed suggest that the boundary lubricant is in a fluidlike (viscous and not Newtonian) state under these conditions. In marked contrast to conventional stick-slip behavior, no stiction spikes are observed on starting the sliding from rest or after reversing the sliding direction. A logarithmic $\sigma(V)$ dependence was observed before with similar boundary lubricants, but under *dry* sliding conditions [35]. However, more recent boundary lubrication studies under dry atmospheres have not found this functional dependence [13,27].

In the smooth-sliding regime at low V, σ levels off at some driving velocity V_1 (crossover velocity), after which it remains roughly constant with increasing V up to the first critical velocity V_{c1}, at which point the smooth-to-stick-slip bifurcation occurs (Fig. 3). At higher shear rate when $V>V_{c2}$, the inverted stick-slip regime transits towards a second smooth-sliding state. The value of the friction force in this second steady state at V_{c2} is lower than at V_{c1}, just before the stick-slip regime. As V increases above V_{c2}, the interfacial friction increases and the mechanical system is restabilized. Over the limited range of velocities, that we can investigate in this second smooth-sliding regime, the shear stress seems to increase linearly with the driving velocity, as shown in Fig. 4.

Depending on the temperature or the type of surfactant and surface densities, only a part of the full σ-V curve, shown in Fig. 3, would be observed over the range of experimental velocities attainable. For example, for the trimeric surfactant at eight times the CMC, during the first hours of adsorption and before saturation adsorption is achieved, we observe the ''high shear rate'' transition. However, after saturation adsorption is reached, high velocity sliding proceeds almost exclusively by the stick-slip motion. This is because the second threshold velocity V_{c2} is shifted to higher values than the maximum experimental driving velocity attainable. To access the second transition at high shear rates, the concentration of the trimeric surfactant was lowered by a factor 10 to just below the CMC. This reduced the surfactant density in the adsorbed bilayers and reduced V_{c2} to easily accessible values (Fig. 3).

The transition at V_{c2} between the smooth sliding and inverted stick-slip regimes characterized by periodic relaxation oscillations of large amplitude, may reveal an intermediary complex time-dependent behavior [15]. A sequence of successive oscillatory states is then observed over a noticeable driving velocity range below V_{c2} at the onset of the transition. The oscillatory states can be either periodic, but with a complex periodic pattern, or aperiodic. Some examples of such time-dependent friction responses are illustrated in Fig. 5, with the corresponding Fourier spectra and phase portraits obtained at different driving velocities. These three-dimensional phase portraits were constructed from measurements of the single available variable [from the time series of the friction force, $F(t)$] by the time delay method, in which $F(t)$ is plotted as a function of $F(t+\Delta t)$ and $F(t+2\Delta t)$, where Δt is fixed [28]. The V dependence of the dynamical behavior can be summarized as follows. Starting from the steady state at a high shear rate, by decreasing V the time-independent state transits to a time-dependent state exhibiting periodic oscillations of smaller amplitude than in the inverted stick-slip regime. The transition is subcritical, i.e., discontinuous first order but with a narrow range of hysteresis. The oscillations appear to be periodic, but the basic pattern consists of two oscillations of different amplitudes, as illustrated in Fig. 5(d). These oscillations are not relaxation oscillations, but rather quasiharmonic oscillations. In this periodic regime, which exists over a narrow range of V, the surfaces never stick together. A further reduction of V leads to an aperiodic oscillatory state, as the one shown in Fig. 5(c). The corresponding power spectra no longer show well-defined peaks, but rather a broadband above the instrumental noise level. This aperiodicity is well illustrated by the corresponding phase portrait [Fig. 5(c)], showing a coarse attractor in contrast to the previous one where the trajectories are contracted on limit cycles [Fig. 5(d)], within the experimental accuracy. A further reduction of V leads to a new periodic state with more complex motifs, as shown in Fig. 5(b). These periodic states are separated by the aperiodic states. Ultimately, the region of complex oscillatory states gives rise to the inverted stick-slip region at lower V, Fig. 5(a).

The scenario described above is sensitive to the applied load. By increasing the compression load, the sequence seems to be *simplified* and the number of different states is reduced. No interpretation of the sequence in terms of dynamic systems can be advanced due to two difficulties: the limited signal-to-noise ratio of the device at high shear rates and limitations of the finite distances sheared during each cycle. Given that the surfaces are rubbed in cycles of about 20 μm in amplitude, the number of oscillations per cycle is restricted and low-frequency components cannot be detected. Moreover, each time the sliding direction is reversed, the system first goes through a transient regime before reaching the oscillatory steady state, since the driving velocity passes through zero during the inversion. The transient regime reduces the number of useful oscillations per cycle which can be sampled for analysis.

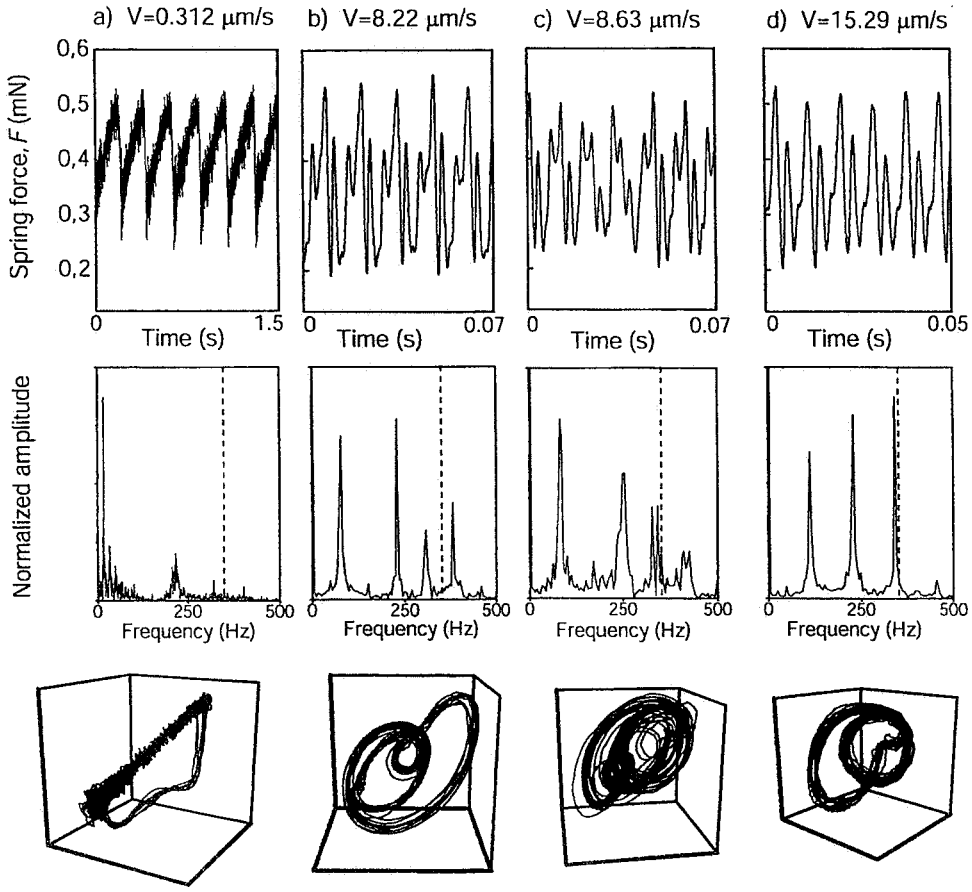

FIG. 5. Measured friction traces, normalized amplitude Fourier spectra, and phase portraits of the spring force at different driving speeds, $L=4.51$ mN and $T=20\,^{\circ}$C. The time delay chosen to build the phase portrait is (a) 10^{-3} s, (b)–(d) 0.5×10^{-3} s. The dotted lines in the Fourier spectra indicates the resonance frequency of the mass-spring system used in this particular experiment (351 Hz).

B. Load dependence

When the surfaces are at rest ($V=0$), the change of the contact area with load over the investigated load range is very well described by the Johnson-Kendall-Roberts (JKR) theory [29], as shown in Fig. 6. Usually, only a weak adhesion hysteresis was found along a loading-unloading cycle. Furthermore, within the resolution of our experimental setup, we did not observe any change in the contact area when the surfaces slide past each other. However, when separated during sliding, the surfaces jumped apart at lower negative loads than when they were not sliding, $V=0$. Therefore, the adhesion is reduced by shearing. Note that for this kind of systems, the measured adhesion energy is relatively weak, around a few mJ/m^2 (Fig. 6), regardless of the surfactant and the temperature [see Fig. 11(b) later], provided that the bulk surfactant concentration is close to or above the CMC.

Figure 7(a) shows the load dependence of the σ-V curve at a fixed temperature. Within the experiment accuracy, the shear stress σ appears to be independent of the normal load L over the range of loads (and contact areas) investigated, both along the plateau regime preceding the stick-slip instability, $V_1>V>V_{c1}$, and for the high velocity smooth-sliding regime when $V>V_{c2}$. This is illustrated in Fig. 8. Note that the load independence is no longer verified along the logarithmic regime when $V<V_1$ [Fig. 7(a)]. At these small velocities, the σ-V curves can be superposed on the same master curve as shown in Fig. 7(b) by plotting σ as a function of V/V_0, where $V_0(L)$ is the intercept with the velocity axis of the logarithmic part of the curves. At a fixed temperature, we find that $-\ln(V_0)$ scales as $L^{1/6}$ for the range of load studied.

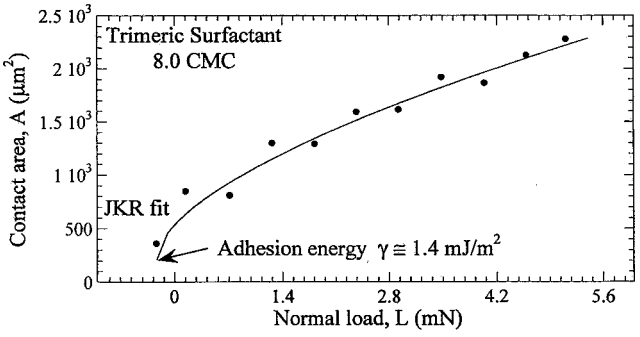

FIG. 6. Contact area as a function of normal load, for loading and unloading of two mica surfaces under a solution of 8 CMC of trimeric surfactant, after hemifusion. The measured data is well described by the Johnson-Kendall-Roberts (JKR) theory of contact mechanics (continuous line) [29].

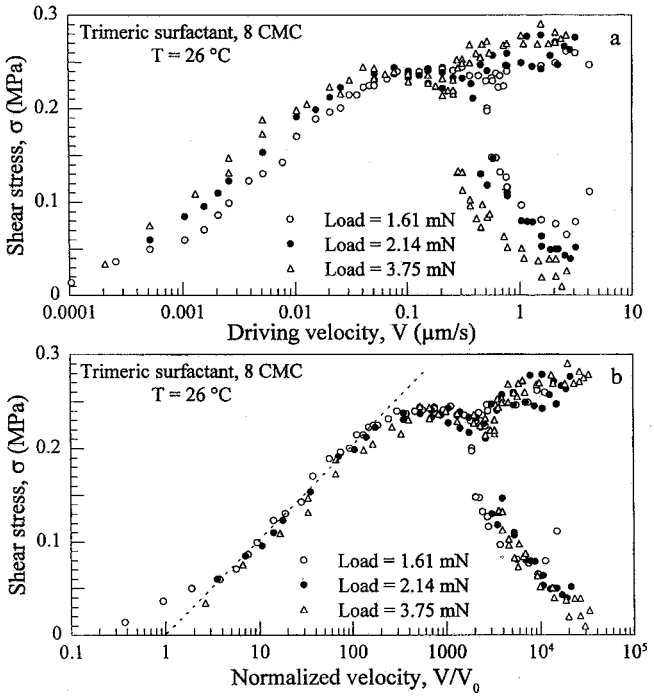

FIG. 7. (a) Sliding-velocity dependence of the shear stress between two adsorbed monolayers of the 12-3-12-3-12 surfactant at different normal loads. $T=26\,^{\circ}\mathrm{C}$. Surfactant concentration 8 CMC. (b) The curves measured are superposed after normalizing the sliding velocity by V_0 (obtained from the intercept of the logarithmic regime, as described in the text).

Since the contact area A scales as $L^{2/3}$ at large loads [29], the friction force has an almost linear load dependence along the logarithmic regime, more precisely $F \propto L^{5/6}$ or $F \propto A^{5/4}$. More systematic investigations are necessary to definitively establish the exact values of these exponents.

The normal load also has a noticeable effect on the first critical velocity V_{c1}. As illustrated in Fig. 9, two regimes can be identified. At very low or negative loads, V_{c1} increases sharply with L. In contrast, at larger loads, V_{c1} decreases weakly with L, i.e., increasing the load at constant V

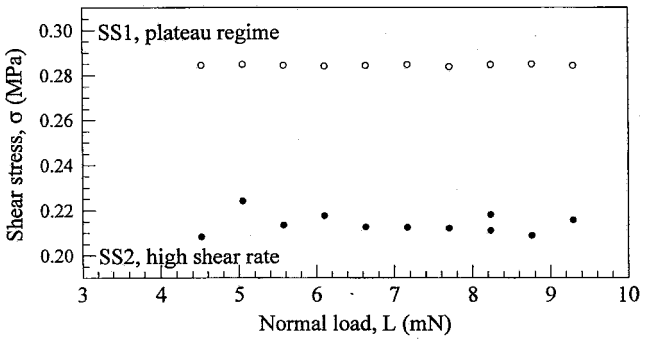

FIG. 8. Load dependence of the shear stress between two adsorbed monolayers of the trimeric 12-3-12-3-12 surfactant in the low velocity (open symbols; $V=0.052\ \mu$m/s) and high velocity (closed symbols; $V=20.8\ \mu$m/s) smooth-sliding steady states. $T=20\,^{\circ}\mathrm{C}$. Surfactant concentration 0.8 CMC.

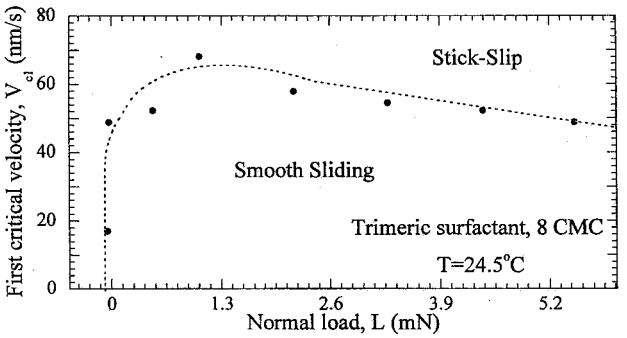

FIG. 9. Bifurcation diagram between the smooth and inverted stick-slip sliding for the 12-3-12-3-12 surfactant for a temperature of $T=24.5\,^{\circ}\mathrm{C}$.

changes smooth sliding into inverted stick-slip sliding. For the second transition at high shear rate, the opposite effect is observed: the higher is the load, the larger is the critical velocity V_{c2}. Thus, increasing the load extends the range of the inverted stick-slip regime.

C. Temperature dependence

Temperature may have important and different effects on the hemifusion process, the force profile (Fig. 2), and the friction forces. For instance, for the 12-3-12-3-12 trimeric surfactant, the hemifusive rupture is no longer triggered by compression at temperatures higher than 24 °C, within the experimental window of accessible loads. However, shearing at driving velocities larger than a certain threshold can induce the hemifusion. Once hemifusion has occurred, the monolayer-monolayer contact is maintained, regardless of the driving velocity. At temperatures larger than 28 °C, the first-order (discontinuous) hemifusion transition is never achieved, even under large loads and fast-sliding velocities. Under such conditions, the bilayers are simply gradually compressed down to a thickness corresponding to two single monolayers. In addition, the contact is no longer adhesive and the friction force is much reduced at all sliding velocities, often below the apparatus sensitivity. This behavior suggests that at these elevated temperatures, the adsorbed surfactant layer changes its physical state (e.g., amorphous to liquidlike).

Figure 10(a) illustrates how the sliding σ-V curve is modified when the temperature is changed under similar loads. An increase of the temperature leads to an increase of the critical velocity V_{c1} and a decrease of the shear stress σ. An example of the dramatic change of σ with temperature is given in Fig. 11(a) in the plateau region of the first smooth-sliding regime (which is only weakly dependent on L and V, as shown in Fig. 7). Interestingly, over the same temperature range the adhesion energy is fairly constant, as shown in Fig. 11(b). These adhesion values were directly measured from the pull-off forces needed to separate the two surfaces from contact [Fig. 2(a)]. Values obtained from the best JKR fit of the contact area-load curves, similar to the one in Fig. 6, are consistently lowered by almost a factor of 2.

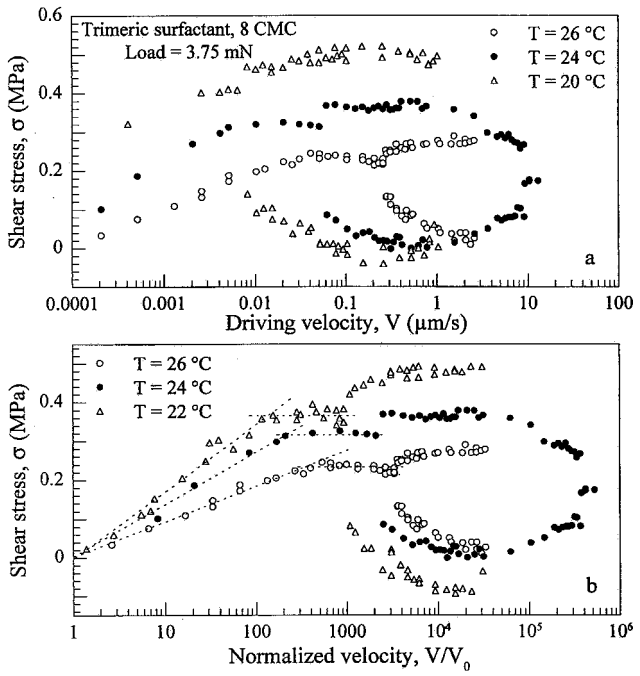

FIG. 10. (a) Sliding-velocity dependence of the shear stress between two adsorbed monolayers of the 12-3-12-3-12 surfactant at different temperatures; normal load $L=3.75$ mN; surfactant concentration 8 CMC. (b) The measured curves do not superpose after normalizing the sliding velocity by V_0 (obtained from the intercept of the logarithmic regime, as described in the text). The translation of the crossover between the logarithmic and the plateau regimes is due to the change of the longer characteristic time with the temperature.

Decreasing the temperature reduced both V_1, the crossover velocity between the logarithmic and the plateau regime, and V_{c1}. In particular, a linear relation was observed between $\ln V_{c1}$ and T^{-1}, as can be observed in Fig. 12.

D. Bulk surfactant concentration dependence

Concentration studies are more time consuming and only a limited number of concentrations were investigated. The following trends were observed.

At low surfactant concentrations, well below the CMC, the friction force was relatively weak and smooth in the velocity range studied (from a few nm/s to a few μm/s). At these low concentrations, the surfaces were covered by patches of monolayer or by an incomplete bilayer. The more concentrated the solution is, the larger is the friction force in the monolayer-monolayer contact, and the lower is the adhesive energy. For instance, with the CTAC surfactant, the inverted stick-slip regime first emerges at concentrations larger than 0.05 CMC when the adsorbed bilayers are not yet fully developed. In this case, the smooth-sliding–to–stick-slip transitions occur at large driving velocities V_{c1}, and the amplitude of the relaxation oscillations in the stick-slip regime is smaller. The more concentrated the solution is, the lower is V_{c1}, and the larger is the stick-slip amplitude. The same trends were found with the trimeric surfactant, as shown in Fig. 13, which compares the sliding curves measured at 0.8 and 8 CMC under similar normal loads.

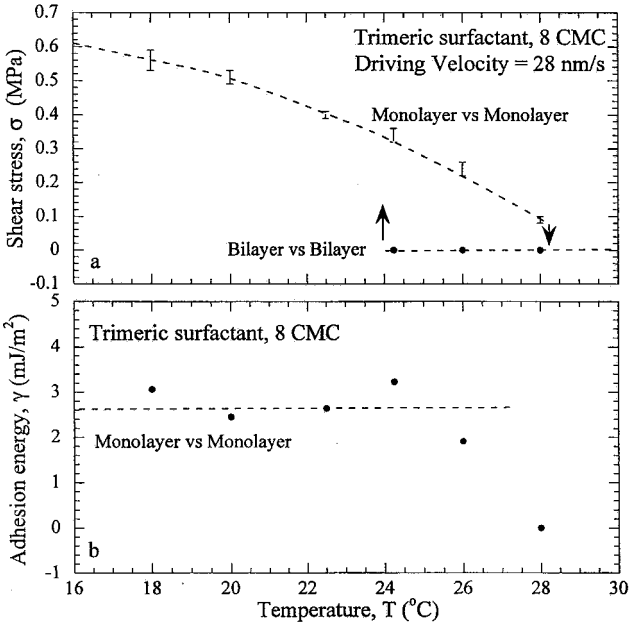

FIG. 11. (a) Change of σ with temperature at a driving velocity corresponding to the first steady state on the plateau regime, $L=1.8$ mN. (b) Temperature dependence of the adhesion energy for the 12-3-12-3-12 surfactant.

In summary, increasing the bulk surfactant concentration has effects similar to those when increasing the normal load or decreasing the temperature: all lead to an increase of the shear stress, a decrease of V_{c1}, and to an extension of the range of the inverted stick-slip regime.

IV. MODEL

The shape of the measured σ-V curves discussed above resembles earlier results presented by Grosh for the sliding of elastomer blocks [30], and more recent results obtained with dialkyl surfactant monolayers [31,32]. In each case, there was a finite value for the adhesion energy between the rubbing surfaces. However, two differences between these and our system have to be remarked. First, the inverted stick-

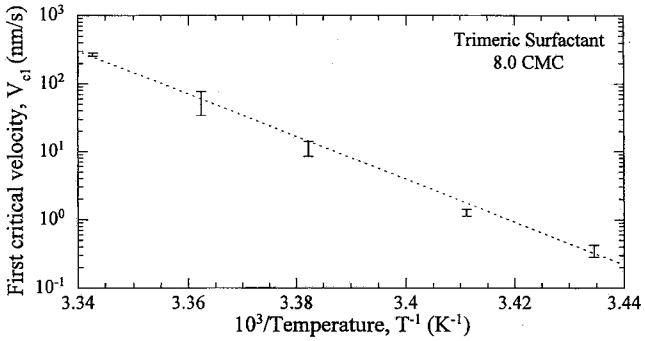

FIG. 12. Dependency of the critical velocity V_{c1} with the inverse of temperature for the 12-3-12-3-12 surfactant, $L=1.8$ mN.

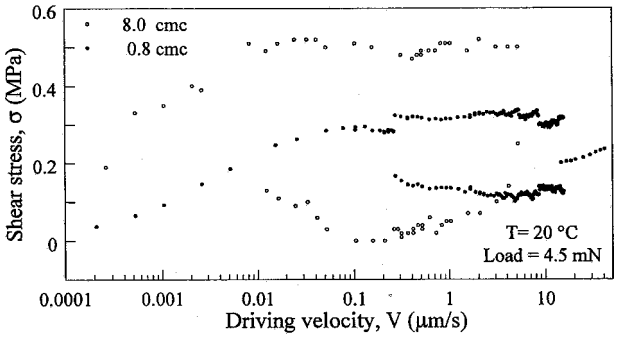

FIG. 13. Sliding-velocity dependence of the shear stress between two adsorbed monolayers of the 12-3-12-3-12 surfactant at two different bulk surfactant concentrations, (open symbols for 8 CMC and closed symbols for 0.8 CMC) at $L=4.5$ mN and $T=20$ °C.

slip behavior was not reported in the previous studies; this may be due to a higher stiffness K_m of their mechanical setup. It is well known that a stick-slip regime exists only over a limited range of the K_m-V phase space [2]. Second, the force plateau may have a very different velocity range in each case: it may even be shortened to a simple peak, as will be discussed below.

The main trends of the σ-V curve presented in Fig. 3 can be accounted for by a theory of adhesive friction, originally developed for ''elastomer'' surfaces [16,33,34], but that can be applied to any sheared surfaces bridged together by any kind of weak adhesive junctions. Let us assume that at any instant, the adhesive area A consists of N independent bonds or adhesive nanodomains, hereafter called ''junctions,'' each of average area δA. During motion, the whole contact area A does not slide as a single unit: individual junctions are continually formed and broken incoherently. Each junction is assumed to stretch elastically up to its breaking or yield point. In the model, a junction detaches either spontaneously, by thermal excitation, or by the external shear force, and reforms further down after various thermoelastic relaxation processes have occurred. Two characteristic times are involved: τ_0, the mean time to *break* a junction due to thermal fluctuations under *zero* lateral stress or local shear force, and τ, the mean time to thermally *activate* or reactivate a junction. Upon shearing, the junctions are elastically deformed, resulting in a reduction of the energy barrier to transit from the bonded to the free state. If the reduction is assumed to be proportional to the elastic force f_{elas}, as proposed by Schallamach [16], the characteristic lifetime of a *stressed* junction becomes $\tau_0 \exp(-\gamma f_{\mathrm{elas}}/k_BT)$, where γ is a constant with the dimension of length. A junction is also always depinned immediately, once the local stress reaches the yield point [33,34]. Let $l^*=Vt_b$ be the critical deformation at the yield point, with $t_b(V)$ as the time to reach this point starting from rest at a given velocity V. It is also assumed that in contrast to the rupture time, the time of junction formation τ is independent of the shear rate, but dependent on temperature.

In this model, the dissipation comes from the elastic energy stored during the deformation of the junctions in the adhesive state and then irreversibly lost (dissipated as heat) when they are depinned. The total friction force can be written as $F=N_0\overline{f}_{\mathrm{elas}}$, where N_0 is the number of junctions in the bonded state depending on V and $\overline{f}_{\mathrm{elas}}$ is the mean elastic force of the adhesive junctions averaged over the contact area. The elastic force per bonded junction is $f_{\mathrm{elas}}=\delta AGVt/d$, where G is the shear modulus, d the thickness of the junction, and t the elapsed time since the zero-stress state.

On solving the above equations, the model predicts four limiting friction regimes, provided that $\tau_0 \gg \tau$. At very low sliding velocity, $V \ll l^*/\tau_0$, the junctions are always broken by thermal fluctuations and the mean lifetime of a junction is close to the static lifetime, $\langle t\rangle_b \cong \tau_0$. The friction is then proportional to the sliding velocity, defining the ''rheological'' or linear V regime [16,33]. The lubricant film behaves similar to a Newtonian fluid, and $\sigma \sim GV\tau_0/d$.

At higher driving velocity, where V becomes comparable with l^*/τ_0, the forced rupture process competes with the thermal mechanism with lowered activation barriers, giving in the first approximation a logarithmic V dependence for the shear stress [34], as is commonly found in a creep regime [2,35,36]. The stress is now given by $\sigma \sim (k_BT/\gamma\delta A)\ln(V/V_0)$, with $V_0=(k_BTd)/(\gamma\delta AG\tau_0)$.

Beyond this regime, where $l^*/\tau \gg V \gg l^*/\tau_0$, the junctions are mainly elastically depinned, reaching the critical stress in an uncorrelated manner. The shear stress is then almost velocity independent [33,34] and given by $\sigma \cong 1/2Gl^*/d$, since the number of junctions in the bonded state is almost constant. Such a behavior arises only if the two characteristic times τ and τ_0 are well separated, $\tau_0/\tau \gg 1$.

Finally, at even higher velocity, as V becomes comparable to or larger than l^*/τ, the number of junctions in the bonded state N_0 decreases, since each junction now spends relatively more and more time in the unbonded state. By definition, $N_0=N\langle t\rangle_b/(\langle t\rangle_b+\tau)$; when $\langle t\rangle_b=t_b=l^*/V<\tau$, then $N_0 \cong Nt_b/\tau$, i.e., N_0 and therefore the shear stress decrease as the inverse of the sliding velocity [33,34], $\sigma \sim V^{-1}$.

If the condition $\tau_0 \gg \tau$ is not satisfied, the σ-V profile predicted by the model is modified to a large extent. For τ_0 comparable to or even smaller than τ, the plateau in the σ-V profile narrows or disappears, leaving a peak where the logarithmic and V^{-1} regimes merge together. The number of junctions in the adhesive state, N_0, starts to decrease when the adhesive junctions are still depinned both by the thermally activated process and by the external shear stress. Several examples of such peaked σ-V curves have been reported in lateral force microscope experiments with adhesive surfactant-coated surfaces [31,32].

The elastic-adhesive model discussed above accounts for the logarithmic and plateau regimes of the experimental σ-V curves (Figs. 3, 7, and 11) and provides an interpretation for the inverted stick-slip bifurcation. At the onset of the $\sigma \propto 1/V$ regime, a mechanical instability may arise when $d\sigma/dV$ becomes negative, i.e., as soon as the number N_0 of junctions in the bonded state starts to significantly decrease at larger velocities.

Within the framework of this model, the experimental

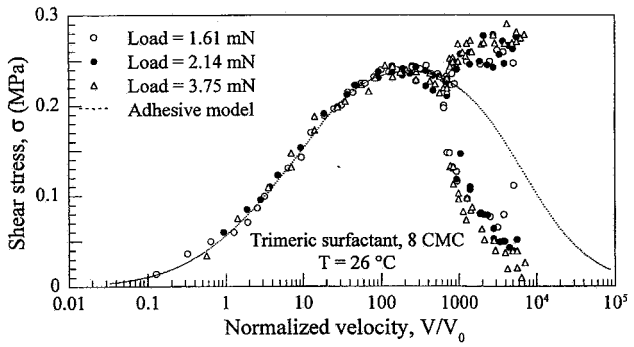

FIG. 14. Sliding-velocity dependence of the shear stress between two adsorbed monolayers of the 12-3-12-3-12 surfactant at different normal loads and $T=26\,^{\circ}\mathrm{C}$. The dotted line is the best fit obtained with the adhesive friction model, as described in the text.

σ-V curve obtained with the trimeric surfactant at a bulk surfactant concentration of 8 CMC and $T=26\,^{\circ}\mathrm{C}$ (Fig. 14) can be remarkably fitted by the following equations (see the Appendix):

$$F_{\mathrm{elas}}=\frac{t_b}{\langle t\rangle_b+\tau}N\frac{k_BT}{\gamma\alpha}\int_1^{e^\alpha}\frac{d\eta}{\eta}\ln(\eta)\exp\left(-\frac{t_b}{\alpha\tau_0}\eta\right),$$

$$\langle t\rangle_b=t_b\exp\left(-\frac{t_b}{\alpha\tau_0}(e^\alpha-1)\right)+\frac{t_b^2}{\alpha^2\tau_0}\int_1^{e^\alpha}d\eta\ln(\eta)\times\exp\left(-\frac{t_b}{\alpha\tau_0}\eta\right), \quad (1)$$

with $\alpha=\gamma\delta AGl^*/dk_BT$. The fit was performed with four free independent parameters τ_0, l^*, G, and $\gamma\delta A$. Knowing the thickness of a monolayer, $d\cong 2$ nm, the numerical values obtained are $l^*=4.5$ Å, $G=2.28$ MPa, $\gamma\delta A=32.8\ \mathrm{nm}^3$, τ_0 between 0.13 and 0.3 s, and τ between 184 and 417 μs (the last two quantities are functions of the applied load). All the fitted values appear to be physically reasonable. The activation volume $\gamma\delta A$ indicates that a junction has an area of approximately $(\gamma\delta A)^{2/3}=10.3\ \mathrm{nm}^2$, i.e., composed of about 20 monomeric molecules.

The elastic-adhesive model described above is insufficient to account for the second steady smooth-sliding regime at larger driving velocities. It predicts that eventually the friction vanishes at high shear rates. A second contribution to the friction force, other than the elastic contribution, must be considered in order to restabilize the mechanical system in a kinetic state with a finite friction. This extra contribution may arise from the free junctions, $N-N_0\sim N(1-l^*/\tau V)$ sliding past each other over an average time of τ. For the surfactant monolayers considered here, we may associate this second contribution to the viscous friction, $F_{\mathrm{vis}}\sim V$, if the monolayers are in a liquidlike state, or to the cost of tilting the molecules during sliding if they are rather in a solidlike state. The linear increase of the force at high sliding velocity (Fig. 4) seems to support the idea of a viscous contribution.

At this stage, we can propose a constitutive friction law for the system considered here:

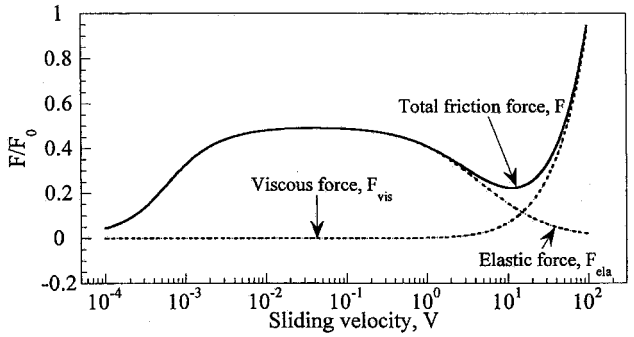

FIG. 15. Representation of the elastic-viscous model for the friction force vs sliding velocity. The viscous contribution is more important at faster driving velocities, while the elastic contribution dominates at slower velocities.

$$F(V)=\phi(V)N\overline{f}_{\mathrm{elas}}(V)+[1-\phi(V)]Nf_{\mathrm{vis}}(V), \quad (2)$$

where ϕ is the fraction of junctions in the bonded state, $\overline{f}_{\mathrm{elas}}$ and f_{vis} are the mean contributions per junction in the adhesive and free states, respectively. Following Chernyak and Leonov [33], a simpler expression for Eq. (1) with a similar qualitative behavior can be derived (see the Appendix). Using this result, Eq. (2) takes then the following analytical expression:

$$F=\phi F_0\frac{V\tau_0}{l^*}\frac{1-(1+l^*/V\tau_0)e^{-l^*/V\tau_0}}{1-e^{-l^*/V\tau_0}}+(1-\phi)\frac{A}{d}\eta V \quad (3)$$

with

$$\phi(V)=\frac{\langle t\rangle_b}{\langle t\rangle_b+\tau}. \quad (4)$$

The mean lifetime of a junction in the bonded state has now a much simpler expression than Eq. (1): $\langle t\rangle_b=\tau_0(1-e^{-l^*/V\tau_0})$. F_0/N is the mean elastic shearing force per junction in the nonthermal regimes, where adhesive junctions are broken only by the external shearing mechanism, $F_0=A/dGl^*$.

Figure 15 shows the elastic-viscous friction force of Eq. (3) as a function of the sliding velocity when the two static characteristic times are well separated, $\tau_0/\tau\gg 1$. As can be observed in the figure, the viscous contribution becomes significant only at large sliding velocities, i.e., when the number of junctions in the free state increases abruptly, $(1-\phi)\,N\sim N(1-l^*/\tau V)$ when $l^*/V\ll\tau\ll\tau_0$. At lower velocities, this number tends to zero; most of the junctions are in the adhesive state and the main contribution to the dissipation comes from the elastic component.

Luengo *et al.* [17] have shown that the equation of motion of the SFA nanotribometer can be reduced to the equation of motion of a block of mass m (upper surfaces of the SFA) sliding on a substrate, the block being connected to an elastic spring of stiffness K_m (double-cantilever spring of the fric-

tion device) which is pulled at one end with velocity V. This can be formalized by the following ordinary differential equation (ODE) system:

$$\dot{x}=\nu,$$
$$m\dot{\nu}=K_m(Vt-x)-F, \tag{5}$$

where x is the instantaneous position of the upper surface. Overdots indicate time derivatives. After combining Eqs. (3) and (5) and some rescaling, Eq. (5) can be written in the dimensionless form

$$\dot{\xi}=\frac{V}{\nu_0}-\nu,$$
$$\dot{\nu}=\xi-2\phi\frac{\nu}{B}\frac{1-(1+B/|\nu|)e^{-B/|\nu|}}{1-e^{-B/|\nu|}}-(1-\phi)A\nu \tag{6}$$

with the fraction of junctions in the adhesive state given by

$$\phi=\frac{1-e^{-B/|\nu|}}{1-e^{-B/|\nu|}+\tau/\tau_0}, \tag{7}$$

where ξ and ν are the dimensionless position and velocity of the upper surface, given by x/x_0 and $\dot{x}/\nu_0$ with $F_0=A/dGl^*=K_mx_0$, $\tau_m=(m/K_m)^{1/2}$, and $\nu_0\tau_m=x_0$, while $B=l^*/\nu_0\tau_0$. Numerical integration of Eq. (6) accounts qualitatively for the inverted stick-slip scenario, i.e., an inverted stick-slip regime with relaxation oscillations bounded by two steady smooth-sliding regimes. The first transition at low V occurs after the friction has reached a plateau on which the strength of the friction force is almost constant. It is out of the scope of this paper to report detailed results on these numerical simulations, which will be presented in a forthcoming paper. We would just like to mention that the dimensionality of Eq. (6) is not high enough to fully account for all the experimental observations. It has only two independent variables, ξ (the position of the block) and $\nu=d\xi/dt$ (its instantaneous velocity). Such a dynamic system has solutions either as steady or periodic oscillatory states, with no complexity in the basic motif (harmonic or relaxation oscillations) [38]. As we have already mentioned, the transition between the steady smooth-sliding regime of high shear rate and the inverted stick-slip regime reveals a sequence of successive oscillatory states either as periodic with a complex periodic pattern or even aperiodic (Fig. 5). The minimal dimension to account for such a complex dynamics is 3 [37].

To increase the dimensionality of the model, a third variable must be added. This has been done in different tribological models by introducing a state variable [2,7,8]. A good candidate for a state variable is ϕ, the fraction of junctions in adhesive state, with a memory effect formalized by a supplementary differential equation. The simplest way to introduce this new variable is

$$\dot{\phi}=\frac{1}{\tau}\phi(1-\phi)-\phi\varphi(\dot{x}), \tag{8}$$

where the function $\varphi(\dot{x})$ must satisfy $1-\phi=\tau\varphi(\dot{x})$ under a stationary condition, i.e., $\varphi(\dot{x})^{-1}=\tau+\tau_0[1-\exp(-l^*/\dot{x}\tau_0)]$ when $\dot{x}=V$. The first term on the right-hand side of Eq. (8) describes the behavior when the surfaces are at rest ($\dot{x}=0$), so that the number of junctions in the adhesive state only depends on the two characteristic times τ and τ_0, $\phi_0=\tau_0/(\tau_0+\tau)$, i.e., $\phi_0\cong 1$ since $\tau_0/\tau\gg 1$. ϕ has two limit values 0 (unstable) and 1 (stable), accounting for the state of the boundary film; 1 stands for adhesive and 0 for nonadhesive. According to Eq. (8), from any initial state with $\phi<1$, the contact will tend to adhere at a characteristic rate proportional to $1/\tau$. A natural choice for this characteristic time is the mean lifetime of the junctions in the free state. Equation (8) introduces a memory effect in the equation of motion for the center of mass (5); the number of junctions in the adhesive state is no longer a variable only of the relative velocity between the two surfaces, $\dot{x}(t)$, but also depends on the previous history of the system. In combining Eqs. (8) and (6), a new dimensionless ODE system can then be written as

$$\dot{\xi}=\frac{V}{\nu_0}-\nu,$$
$$\dot{\nu}=\xi-2\phi\frac{\nu}{B}\frac{1-(1+B/|\nu|)e^{-B/|\nu|}}{1-e^{-B/|\nu|}}-(1-\phi)A\nu, \tag{9}$$
$$\dot{\phi}=\frac{\tau_0}{\tau}\phi(1-\phi)-\frac{\tau_0\phi}{\tau_0(1-e^{-B/|\nu|})+\tau}.$$

Numerical integration of Eq. (9) produces solutions with more complex time-dependent behaviors than the ones found with Eq. (6). Oscillatory states with basic patterns including successive oscillations of large and small amplitudes can be observed at the onset of the transition to the steady state of high shear rate. Some of them can even transit into a chaotic state by a subharmonic cascade [39] or type-III intermittency [40] scenario. However, even if there exist strong similarities between the dynamic states of the model and the experimental results, up to now we have failed to find a set of parameters generating a sequence with a large number of complex oscillatory states over a restricted range of driving velocity, as observed along the experimental σ-V curve shown in Fig. 3.

V. DISCUSSION

The proposed adhesive friction model describes the friction behavior of boundary-lubricated surfaces and provides an interpretation for the physical origin of the observed inverted stick-slip. This is caused by the mechanical instability occurring when the friction force decreases with increasing driving velocity. The striking feature of this system comes from the fact that two steady smooth-sliding states surround the stick-slip regime, with the one at low sliding velocity involving thermally activated processes. Such thermal processes are commonly invoked to account for the behavior of many macroscopic tribological systems. However, they are usually associated with aging effects [7,41], such as the increase of the real contact area of asperities by plastic creep,

generating an opposite effect of increasing stress when the sliding velocity decreases, and resulting in high static friction. In contrast, the adhesive model described above, with a thermal process of rupture of adhesive junctions, predicts a zero static friction force followed by a linearly increasing friction with driving velocity, as was found experimentally.

As already mentioned, the model has two characteristic times τ_0 and τ, and a characteristic length l^*. The characteristic time of thermal rupture of a junction, τ_0, is important only at very low shear rates where the adhesive junctions are broken mainly by thermal fluctuations. When the rupture mechanism by the external force becomes dominant, the mean lifetime of the adhesive junctions is determined by the characteristic length, $\langle t \rangle_b = l^*/V$. Thus, for the nonthermal regimes (plateau, stick slip, and second steady state), the model is completely defined by one characteristic time and a characteristic length.

According to the model, the larger is the ratio τ_0/τ, the larger is the plateau regime, and therefore larger is the stick-slip range. Experimentally, the range of the stick-slip regime increases at higher loads or bulk surfactant concentrations. It seems physically reasonable that an increase of the load causes an increase of the time ratio τ_0/τ, because the larger is the load, the longer will be the time to thermally break an adhesive junction, and the shorter will be the time to thermally reactivate a broken one. Figure 7(b) illustrates the increase of τ_0 with the load. In order to put the data on the same σ-V master curve, the driving velocities were normalized by V_0, as described in Sec. III. According to the model, $V_0 = l^*/(\alpha\tau_0)$; α can be obtained graphically at the crossover between the logarithmic and the plateau regimes, $\alpha = \ln(V_1/V_0)$. We found that V_0 decreases with increasing load. The existence of a master curve indicates that α as well as l^* (related to the plateau value) and the activation volume $\gamma\delta A$ (or the junction size, related to the slope of the logarithmic part) are independent of the load. Therefore, according to the model, the decrease of V_0 is merely due to an increase of τ_0 with increasing load.

The bulk surfactant concentration dependence illustrated in Fig. 13 is more difficult to account for. One of the problems is the enlargement of the stick-slip range that occurs with the increase of the shear stress. At low concentrations, the friction is relatively weak and no stick-slip is ever observed. Within the framework of the model, we may invoke different causes for such a dependence. Maybe the local shear modulus becomes increasingly stiffer as the surfactant coverage of the surfaces increases. At small surfactant concentrations, due to the low level of the friction force compared to the stiffness of the device, the mechanical stick-slip instability does not occur. Another possible explanation is that at rest, the number of adhesive junctions changes notably with the bulk surfactant concentration, while the adsorbed layers are not fully completed. Under these conditions, only a fraction of the contact area is in the adhesive state. It is equivalent to considering again the ratio of the two characteristic times, $\tau_0/\tau \approx 1$. When the adsorbed monolayers are not yet completed, the mean lifetime in a free state may be longer before the two moieties of a future junction get into a right location and conformation in order to activate it. This seems to be in contradiction with the fact that at small bulk concentrations, the adhesion between the surfactant-bearing surfaces is rather large, often larger by one order of magnitude than that when the adsorbed films are completed. However, this change in adhesion energy is mainly due to the defect loop around the monolayer-monolayer contact. The defect energy scales as the radius of the loop, i.e., the radius of the monolayer-monolayer contact r. Thus, the defect loop opposes the adhesive monolayer-monolayer contact. The more complete the bilayers are, the larger is the line energy due to the loop, and the easier it will be to pull apart the two surfaces. The defect loop has a significant contribution to the adhesion force, but not to the friction force, since the latter scales either as r^2 (plateau, stick-slip, and viscous regime) or $r^{5/2}$ (logarithmic regime) and not as r (see Figs. 7 and 8; r is the radius of the loop).

Figure 12 shows that the first critical velocity V_{c1} scales like $\exp(-\Delta/k_BT)$, which may be expected, given that the observed behavior is interpreted in terms of thermally driven processes. In the framework of the simplest two-dimensional (2D) mechanical model (5), the instability of the first steady state may occur as soon as the friction force decreases with increasing velocity ($dF/dV_s = 0$). By considering only the elastic contribution to the friction force (1),—at the onset of the stick-slip instability, the viscous contribution of the friction force can be neglected, $\phi(V_{c1}) \cong 1$ when $\tau_0/\tau \gg 1$—the first critical velocity can be approximated as

$$V_{C1} \cong \left(\frac{\alpha - 2}{\alpha^3} e^{\alpha} \right)^{1/2} \frac{l^*}{(\tau\tau_0)^{1/2}}.$$

By definition, τ and τ_0 can be written as $\tau^* \exp(U/k_BT)$ and $\tau^* \exp(U_0/k_BT)$, respectively, where U and U_0 are the corresponding energy barriers to be overcome in order to activate or deactivate an adhesive junction. For an overall adhesive system, as the one considered here, $U_0 \gg U$. From the slope of $\ln(V_{c1}) - T^{-1}$ curve, the energy barrier U_0 could be extracted, provided that only τ_0 changes with temperature. This is not the case, since τ, l^*, and α also change. For instance, Fig. 10(b) shows how α systematically changes with temperature. The larger is the temperature, the smaller is α.

Alternatively, the activation energy U_0 could be extracted from the previous V_1 relationship, provided that the temperature changes of α and l^* are known, since by definition $V_0 = l^*/(\alpha\tau_0)$, thence $V_1 \cong (e^{\alpha}/\alpha)(l^*/\tau_0)$. Unfortunately, the barrier energy values obtained either with V_{c1} or V_1 have a strong (exponential) dependence on α, and this quantity is determined with poor accuracy, especially at low temperatures where the logarithmic regime is experimentally restricted. Moreover, the determination of the temperature change of l^* is even less accurate, since l^* can only be measured by fitting the whole σ-V curve; as mentioned before, it involves the fitting of four parameters. Given these limitations, no attempt has been pursued to calculate the energy barrier.

As we have already mentioned, mica surfaces coated by a monolayer of surfactant sliding past each other in dry atmosphere exhibit only a regular stick-slip behavior. This has been reported several times in the past [4,20]. We have found

that with the same pair of surfaces, an inverted stick-slip can be observed when they slide in solution, while regular stick-slip is found when they slide in air, as demonstrated in Fig. 1. Even though in the dry case the surfaces are still coated by a monolayer of surfactant molecules, its molecular density is likely to be different from that of the hemifused monolayers in solution. Nevertheless, the surfaces still make an adhesive contact in dry atmosphere with junctions built with the same material.

Can the previous adhesive friction model still account for this more commonly observed behavior? Let us assume that τ_0 and τ are very large, so that l^*/τ_0 is outside the driving velocity range accessible by the experiment. As a result, an adhesive junction would never be depinned by thermal fluctuations, but is always broken by the imposed external deformation. In addition, let us assume that the characteristic time to form a junction is large enough so that $\tau V/l^* \geqslant 1$; adhesive junctions will then be formed over a significant time, leading to some aging effects resulting in a static friction. The longer the contact stays at rest, the larger would be the number of junctions in the adhesive state, N_0. Besides, the slower is the driving velocity, the larger is $N_0 \cong N l^*/V\tau$, and the larger is the friction force. This aging inducing a static friction generates the common stick-slip scenario. Yamada and Israelachvili [27] have reported such aging effects for the friction between adhesive fluorocarbon surfactant monolayers in dry atmosphere. In the new scenario, the two thermal regimes—linear and logarithmic—do not appear; the thermal fluctuations do not have any effect and the adhesive junctions are always mechanically broken. The regular stick-slip scenario will start somewhere at the onset or inside the fourth regime ($\sigma \sim V^{-1}$) with $N_0(V) < N$ and $dN_0(V)/dV < 0$.

Even if the elastic-viscous model (3) properly describes the inverted stick-slip scenario and, particularly, the five different regimes emerging from the experimental σ-V curves as well as their temperature and load behavior, some questions remain unanswered. It is not straightforward to guess what controls the nanometric elastic coherence length defining the individual junctions, or why this length does not depend on the sliding velocity, as assumed in the model. On the other hand, the assumption that the junctions are independent of each other seems unrealistic, at least nearest-neighbor junction interactions could be expected. A model with only one characteristic time is then open to criticism. One of the main defects of the model is that it does not consider the contact mechanics [42]. The surface geometry of the SFA nanotribometer corresponds to two cylinders mounted on a crossed configuration, so that the distribution of the normal pressure along the circular contact area is nonuniform: the pressure peaks at the center and vanishes at the rim or even becomes negative for adhesive contact [42]. As discussed above, we have found that τ_0 is dependent on the load. Even though the analysis has been done within the framework of a uniformly distributed load, this result appears credible from a physical point of view. The larger the normal loads are, the larger is the characteristic time. We may then conclude that the real peaked distribution of the normal pressure should also imply a radial distribution of the static mean lifetime $\tau_0(r)$ of junctions in the adhesive state. The adhesive junctions would then thermally break more frequently near the edge of the contact area than at the center. Theoretical and numerical studies in this direction may be revealing; this contact-mechanics aspect of the problem is generally neglected in nanotribological analyses.

VI. CONCLUSION

In this paper, we have reported the sliding behavior of adhesive surfactant-bearing surfaces. When the surfaces are fully immersed in an aqueous solution, the dynamic behavior is richer than the one usually observed under dry conditions. On the whole, five different regimes have been identified and accounted for by an extension of the adhesive model of the friction force, initially proposed by Schallamach [16]. The new steady-state, smooth-sliding regimes occurring at low-sliding velocities and preceding the stick-slip regimes are accounted for by a thermally activated process, locally depinning the two adhering surfaces. We have examined how the different regimes depend on the normal load, the temperature, and the bulk surfactant concentration. Under certain conditions, we have found that the oscillatory stick-slip regime exhibits very complex dynamics, implying that such tribological systems must have at least three degrees of freedom. To theoretically describe it, a third independent variable must be introduced into the usual 2D mechanical model, consisting of the equation of motion of a block sliding on a track, being pulled at a constant driving velocity via a spring. The fraction of nanodomains in an adhesive state in the contact region could be this third variable represented by a state variable with a memory.

Even though these results have been obtained exclusively with surfactant-coated surfaces, they can probably be generalized. The model used to describe the data should be broadly relevant for other surfaces in the adhesive contact with local dynamic junctions formed by macromolecules, such as polymer chains or proteins. Many examples can be identified in biological systems.

ACKNOWLEDGMENTS

This work was supported by grants from the U.S. Department of Energy (Grant No. DE-FG03-87ER 45331) and the Keck Foundation. C.D. acknowledges the financial support of INTEVEP, SA.

APPENDIX

1. Derivation of Eq. (1)

At rest, $V=0$, the probability $\hat{P}_0$ for an adhesive junction to stay in this state during the time $(0,t)$ is

$$\hat{P}_0(t) = \exp\left(-\frac{t}{\tau_0}\right), \tag{A1}$$

where τ_0 is a function of temperature, given as

$$\tau_0 = \tau^* \exp\left(\frac{U_0}{k_B T}\right), \tag{A2}$$

with τ^* being an elementary time and U_0 the energy barrier to be overcome for breaking an adhesive junction. The probability that the breakoff then occurs during the same period is

$$P_0 = 1 - \hat{P}_0(t) = 1 - \exp\left(-\frac{t}{\tau_0}\right). \tag{A3}$$

The probability density for thermal breakdown of an adhesive junction at time t is

$$\psi_0(t) = \frac{dP_0}{dt} = \frac{1}{\tau_0}\exp\left(-\frac{t}{\tau_0}\right). \tag{A4}$$

Therefore, the mean time for which an adhesive junction stays bounded is

$$\langle t\rangle_{0b} = \int_0^\infty t\psi_0(t)dt = \tau_0. \tag{A5}$$

In a similar way, we can define the mean lifetime of a free junction,

$$\langle t\rangle_{0f} = \int_0^\infty t\psi(t)dt = \tau, \tag{A6}$$

where $\psi(t)$ is the probability density for a free junction to adhere again. The mean number N_0 of junctions in an adhesive contact per unit of nominal contact area is given by

$$N_0 = N\frac{\langle t\rangle_{0b}}{\langle t\rangle_{0b} + \langle t\rangle_{0f}} = N\frac{\tau_0}{\tau_0 + \tau}, \tag{A7}$$

where N is the total number density of junctions.

Let us now consider how the previous formulas are modified when the two surfaces slide past each other at a finite relative velocity V. During sliding, the adhesive junctions are elastically stressed, resulting in a reduction of the energy barrier to transit from the bonded to the free state. If the reduction is assumed to be proportional to the elastic force $F_e = \delta AGVt/d$, as proposed by Schallamach [16], $U = U_0 - \gamma F_e$, where γ is a constant with the dimension of length and G the shear modulus, δA and d the area and the thickness of junctions, and t the time elapsed since the zero-stress state. Under shear, the lifetime of an adhesive junction is then

$$\tau(V,t) = \tau^* \exp\left(\frac{U_0 - \gamma F_e}{k_B T}\right) \tag{A8}$$

and the survival probability $\hat{P}_V$ for an adhesive junction formed at time $t=0$,

$$\hat{P}_V(t) = \exp\left[-\frac{1}{\tau_0}\int_0^{dt} dt \exp\left(\frac{\gamma\delta AGVt/d}{k_B T}\right)\right]. \tag{A9}$$

The probability of the opposite event is then $P_V(t) = 1 - \hat{P}_V(t)$.

In addition, we assume that an adhesive junction is also depinned when the local stress reaches a critical value or a yield point. Let $l^* = Vt_b$ be the critical deformation at the yield point, with $t_b(V)$ as the time to reach this point starting from rest at a given velocity V. For $t > t_b$, the transition to the free state is certain to occur; therefore, the survival probability of the adhesive junction becomes zero. In assuming that the two breaking mechanisms are independent, the survival probability can be rewritten as

$$\hat{P}_V(V,t,l^*) = \exp\left[-\frac{t_b}{\alpha\tau_0}(e^{\alpha/t_b} - 1)\right]\theta(t_b - t), \tag{A10}$$

where $\theta(x)$ is the Heaviside step function, equal at 1 for $x > 0$ and 0 for $x < 0$, while $\alpha = \gamma\delta AGl^*/dk_B T$. The probability density for an adhesive junction to be depinned then takes the following form:

$$\psi_0(V,t,l^*) = \frac{d}{dt}P_V(V,t,l^*),$$

$$\psi_0(V,t,l^*) = \exp\left(-\frac{t_b}{\alpha\tau_0}(e^{\alpha/t_b} - 1)\right) \times\left(\frac{\theta(t_b - t)}{\tau_0}e^{\alpha/t_b} + \delta(t_b - t)\right). \tag{A11}$$

The mean lifetime of an adhesive junction according to Eq. (A5) becomes

$$\langle t\rangle_b = \frac{1}{\tau_0}\exp\left(-\frac{t_b}{\alpha\tau_0}\right)\int_0^{t_b} t\exp(\alpha t/t_b)\exp\left(-\frac{t_b e^{\alpha/t_b}}{\alpha\tau_0}\right)dt + t_b\exp\left(-\frac{t_b}{\alpha\tau_0}(e^\alpha - 1)\right); \tag{A12}$$

by defining $\eta = \exp(\alpha t/t_b)$, Eq. (A12) can be written like in Eq. (1):

$$\langle t\rangle_b = t_b\exp\left(-\frac{t_b}{\alpha\tau_0}(e^\alpha - 1)\right) + \frac{t_b^2}{\alpha^2\tau_0}\int_1^{e^\alpha} d\eta\ln(\eta) \times\exp\left(-\frac{t_b}{\alpha\tau_0}\eta\right). \tag{A13}$$

In this model, the dissipation comes from the elastic energy stocked during the shearing of junctions in the adhesive state and then definitively lost when they are depinned. Following Chernyak and Leonov [33], the total shear stress can be written as

$$\sigma = \frac{N}{\langle t\rangle_b + \langle t\rangle_f}\int_0^\infty F_e(t)\hat{P}_V(V,t,l^*)dt. \tag{A14}$$

It is assumed that the mean lifetime of a junction in the free state is independent of V, the sliding having no perturbation on the junction formation mechanism. This seems reasonable

at low sliding velocity; $\langle t\rangle_f = \tau$, regardless of V. By combining Eq. (A10) and (A14), we obtain

$$\sigma = \frac{N}{\langle t\rangle_b + \tau}\frac{k_B T}{\gamma t_b}\alpha \exp(t_b/\alpha\tau_0)\int_0^{t_b} t \exp\left(-\frac{t_b}{\alpha\tau_0}e^{t_b/\alpha\tau_e}\right)dt, \tag{A15}$$

and using the change of variables $\eta = \exp(\alpha t/t_b)$, Eq. (A12) can be written like in Eq. (1):

$$\sigma = \frac{t_b}{\langle t\rangle_b + \tau} N \frac{k_B T}{\gamma\alpha}\int_1^{e^\alpha}\frac{d\eta}{\eta}\ln(\eta)\exp\left(-\frac{t_b}{\alpha\tau_0}\eta\right). \tag{A16}$$

Let us consider the different limits.

Linear regime. At very low sliding velocities V, $t_b/\tau_0 \gg 1$. Since $\alpha > 1$, we have both $e^\alpha t_b/\alpha\tau_0 \gg 1$ and $t_b/\alpha\tau_0 \gg 1$. This leads to

$$\hat{P}_V(V,t,l^*) \approx \exp\left(-\frac{t}{\tau_0}\right),$$

$$\langle t\rangle_b \approx \tau_0. \tag{A17}$$

The external shearing force does not contribute to the breaking of adhesive junctions, and the resulting shear stress increases linearly with the sliding velocity,

$$\sigma \approx N\frac{\delta A}{d} G V \tau_0. \tag{A18}$$

Nonthermal regimes. On the other hand, at very large sliding velocities, $t_b/\tau_0 \ll 1$; thence, $e^\alpha t_b/\alpha\tau_0 \ll 1$ and $t_b/\alpha\tau_0 \ll 1$. It is straightforward to show that

$$\hat{P}_V(V,t,l^*) \approx \theta(t_b - t),$$

$$\langle t\rangle_b \approx t_b. \tag{A19}$$

The depinning of adhesive junctions is always due to the external applied force; the thermal fluctuations no longer participate in the process. When $l^*/V \gg \tau$, the net shear stress is almost constant. At this *plateau regime*,

$$\sigma \approx \frac{1}{2} N \frac{\delta A}{d} G l^*. \tag{A20}$$

At larger driving velocities, $l^*/V \ll \tau$, the shear stress decreases with $1/V$,

$$\sigma \approx \frac{l^*}{2V\tau} N \frac{\delta A}{d} G l^*. \tag{A21}$$

Logarithmic regime. For intermediate velocities, where $e^\alpha t_b/\alpha\tau_0 \gg 1$ but $t_b/\alpha\tau_0 \ll 1$, the thermal fluctuation and the external shear force mechanisms contribute together to the breaking of adhesive junctions. The mean lifetime of an adhesive junction (A13) reduces to

$$\langle t\rangle_b \approx \frac{t_b^2}{\alpha^2\tau_0}\int_1^{e^\alpha} d\eta \ln(\eta)\exp\left(-\frac{t_b}{\alpha\tau_0}\eta\right), \tag{A22}$$

which can be expressed in terms of exponential integral functions

$$\int_1^{e^\alpha} d\eta \ln(\eta)\exp\left(-\frac{\eta}{\xi}\right) = -\xi\left[\alpha\exp\left(-\frac{e^\alpha}{\xi}\right) - E_i\left(-\frac{e^\alpha}{\xi}\right) + E_i\left(-\frac{1}{\xi}\right)\right], \tag{A23}$$

with the following expansions when $1/\xi = \alpha\tau_0/t_b \ll 1$ and $e^\alpha/\xi \gg 1$:

$$E_i\left(-\frac{e^\alpha}{\xi}\right) \cong \exp\left(-\frac{e^\alpha}{\xi}\right)(\xi e^{-\alpha} + \xi^2 e^{-2\alpha} + \xi^3 e^{-3\alpha} + \cdots),$$

$$E_i\left(-\frac{1}{\xi}\right) \cong \ln\left(\frac{1}{\xi}\right) + \gamma_E - \frac{1}{\xi}, \tag{A24}$$

where γ_E is the Euler constant. We find then that integral (A23) can be approximated by

$$\int_1^{e^\alpha} d\eta \ln(\eta)\exp\left(-\frac{\eta}{\xi}\right) \approx 1 + \xi(\ln\xi - \gamma_E), \tag{A25}$$

and the mean lifetime of an adhesive junction by

$$\langle t\rangle_b \approx \frac{t_b}{\alpha\tau_0} e^{t_b/\alpha\tau_0} \ln\frac{\alpha\tau_0}{t_b}\left(1 - \frac{\gamma_E - t_b/\alpha\tau_0}{\ln\frac{\alpha\tau_0}{t_b}}\right). \tag{A26}$$

In order to estimate the shear stress (A23), let $\eta = \mu e^\alpha$, so that

$$\int_1^{e^\alpha}\frac{d\eta}{\eta}\ln\eta\exp\left(-\frac{t_b}{\alpha\tau_0}\eta\right) = \int_{e^\alpha}^1 \frac{d\mu}{\mu}(\ln\mu + \alpha)\exp\left(-\frac{t_b e^\alpha}{\alpha\tau_0}\mu\right). \tag{A27}$$

Since $\exp(\alpha) \gg 1$ and $e^\alpha t_b/\alpha\tau_0 \gg 1$, integral (A27) I can be accurately approximated by

$$I = \int_{e^\alpha}^1 \frac{d\mu}{\mu}(\ln\mu + \alpha)\exp\left(-\frac{t_b e^\alpha}{\alpha\tau_0}\mu\right) = \int_{e^{-\alpha}}^{C(t_b e^\alpha/\alpha\tau_0)} \frac{d\mu}{\mu}(\ln\mu + \alpha), \tag{A28}$$

where C is a constant slightly smaller than 1. The asymptotic result is then

$$I \approx \tfrac{1}{2}\ln^2(\alpha\tau_0/t_b). \tag{A29}$$

If $\langle t\rangle_b \gg \tau$, the net shear stress has the following logarithmic dependence:

$$\sigma \approx \frac{1}{2}\frac{k_B T}{\gamma \delta A}\ln(V/V_0), \tag{A30}$$

with $V_0=(k_B T d)/(\gamma \delta A G \tau_0)$.

2. Derivation of the elastic force in Eq. (3)

In this simpler model, it is assumed that the spontaneous breaking of adhesive junctions by thermal fluctuations is independent of the external shearing force, i.e., the activation barrier is not reduced by the local shear stress. The forced breakoff is always assumed to occur at a yield point defined by l^*. The survival probability (A10) can be written as

$$\hat{P}_V(V,t,l^*)=\exp\left(-\frac{t}{\tau_0}\right)\theta(t_b-t), \tag{A31}$$

while the probability density for an adhesive junction to be depinned takes the following form:

$$\psi_0(V,t,l^*)=\exp\left(-\frac{t}{\tau_0}\right)\left(\frac{\theta(t_b-t)}{\tau_0}+\delta(t_b-t)\right), \tag{A32}$$

with $t_b=l^*/V$. The mean lifetime of an adhesive junction according to Eq. (A5) becomes

$$\langle t\rangle_b=\tau_0\left[1-\exp\left(-\frac{t_b}{\tau_0}\right)\right]. \tag{A33}$$

By combining Eqs. (A14) and (A31), the total shear stress can be written as

$$\sigma=\frac{N}{\langle t\rangle_b+\tau}\frac{GV}{d}\int_0^{t_b} t\exp(-t/\tau_0)dt \tag{A34}$$

leading to the following expression:

$$\sigma=\frac{\langle t\rangle_b}{\langle t\rangle_b+\tau}N\frac{GV\tau_0}{d}\frac{1-(1+t_b/\tau_0)e^{-t_b/\tau_0}}{1-e^{-t_b/\tau_0}}, \tag{A35}$$

with $\phi(V)=\langle t\rangle_b/(\langle t\rangle_b+\tau)$. By defining $F_0=NAGl^*/d$, where A is the nominal contact area, the net elastic force has the following form:

$$F_{\mathrm{elas}}=\phi F_0\frac{V\tau_0}{l^*}\frac{1-(1+t_b/\tau_0)e^{-l^*/V\tau_0}}{1-e^{-l^*/V\tau_0}}. \tag{A36}$$

Qualitatively, the shear stress corresponding to Eq. (A36) is similar in shape to the previous stress (A16), with four regimes. Since the coupling between the fluctuation breakoff and the local shear stress is differently treated, the more noticeable difference between the two models arises in the intermediate logarithmic regime. Otherwise, the linear, the plateau, and the $1/V$ regimes are hardly discernible.

[1] E. Rabinowicz, *Friction and Wear of Materials* (Wiley, New York, 1965).

[2] B. N. J. Persson, *Sliding Friction: Physical Principles and Applications* (Springer, Heidelberg, 1998).

[3] A. Berman, W. Ducker, and J. Israelachvili, Langmuir **12**, 4559 (1996).

[4] H. Yoshizawa and J. Israelachvili, J. Phys. Chem. **97**, 11 300 (1993).

[5] A. Berman, W. Ducker, and J. Israelachvili, in *Physics of Sliding Friction*, edited by B. Persson and E. Tosati (Kluwer Academic, Dordrecht, 1996).

[6] A. Berman and J. Israelachvili, *CRC Handbook of Micro/Nanotribology*, edited by B. Bhushan (CRC Press, Boca Raton, 1999).

[7] J. R. Rice and A. L. Ruina, J. Appl. Mech. **105**, 343 (1983).

[8] J. M. Carlson and A. A. Batista, Phys. Rev. E **53**, 4153 (1996).

[9] P. A. Thompson and M. O. Robbins, Science (Washington, DC, U.S.) **253**, 916 (1991).

[10] U. Landman, W. D. Luedtke, and E. M. Ringer, Wear **153**, 3 (1992).

[11] J. N. Glosli and G. Mcclelland, Phys. Rev. Lett. **70**, 1960 (1993).

[12] A. Homola, J. Israelachvili, M. L. Gee, and P. Mcguiggan, J. Tribol. **111**, 675 (1989).

[13] H. Yoshizawa, Y. L. Chen, and J. Israelachvili, J. Phys. Chem. **97**, 4128 (1993).

[14] P. Richetti, C. Drummond, J. Israelachvili, M. In, and R. Zana, Europhys. Lett. **55**, 653 (2001).

[15] C. Drummond, J. Elezgaray, and P. Richetti, Europhys. Lett. **58**, 503 (2002).

[16] A. Schallamach, Wear **6**, 375 (1963); **17**, 301 (1971).

[17] G. Luengo, F.-J. Schmitt, R. Hill, and J. Israelachvili, Macromolecules **30**, 2482 (1997).

[18] M. In, in *Reactions and Synthesis in Surfactant Systems*, Surfactant Series Vol. 100, edited by J. Tetxer (Dekker, New York, 2001), pp. 59–110; V. Bec, O. Aguerre-Chariol, and R. Zana, Langmuir **16**, 141 (2000).

[19] S. Manne *et al.*, Langmuir **13**, 6382 (1997).

[20] H. N. Patrick, G. G. Warr, S. Manne, and I. A. Aksay, Langmuir **15**, 1685 (1999).

[21] R. E. Lamont and W. A. Ducker, J. Am. Chem. Soc. **120**, 7602 (1998).

[22] G. G. Warr, Curr. Opin. Colloid Interface Sci. **5**, 88 (2000).

[23] R. M. Pashley and J. N. Israelachvili, Colloids Surf. **2**, 169 (1981).

[24] J. Israelachvili, *Intermolecular and Surface Forces* (Academic, San Diego, 1992).

[25] U. Raviv and J. Klein, Science (Washington, DC, U.S.) **297**, 1540 (2002).

[26] C. A. Helm, J. Israelachvili, and P. Mcguiggan, Biochemistry **31**, 1794 (1992).

[27] S. Yamada and J. Israelachvili, J. Phys. Chem. B **102**, 234 (1998).

[28] F. Takens, in *Dynamical Systems and Turbulence*, Lecture

Notes in Mathematics Vol. 898, edited by D. A. Rand and L. S. Young (Springer, Berlin, 1981).
[29] K. L. Johnson, K. Kendall, and A. D. Roberts, Proc. R. Soc. London, Ser. A **324**, 301 (1971).
[30] K. A. Grosh, Proc. R. Soc. London, Ser. A **274**, 21 (1963).
[31] Y. Liu, D. F. Evans, Q. Song, and D. W. Grainer, Langmuir **12**, 1235 (1996).
[32] A. Subbotin, G. Hadziioannou, P. R. Ashon, J. A. Preece, and E. W. van der Vegte, Langmuir **16**, 3249 (2000).
[33] Y. B. Chernyak and A. I. Leonov, Wear **108**, 105 (1986).
[34] B. N. J. Persson, Phys. Rev. B **51**, 13 568 (1995).
[35] B. J. Briscoe and D. C. B. Evans, Proc. R. Soc. London, Ser. A **380**, 389 (1982).
[36] T. Baumberger, P. Berthoud, and C. Caroli, Phys. Rev. B **60**, 3928 (1999).
[37] D. Ruelle, Math. Intell. **2**, 126 (1980).
[38] M. Klein and G. Baier, *A Chaotic Hierarchy*, edited by G. Baier and M. Klein (World Scientific, Singapore, 1991).
[39] M. J. Feigenbaum, J. Stat. Phys. **19**, 25 (1978); **21**, 669 (1979).
[40] P. Manneville and Y. Pomeau, Phys. Lett. **A75**, 1 (1979).
[41] A. Ruina, J. Geophys. Res. **88**, 10 359 (1983).
[42] K. L. Johnson, *Contact Mechanics* (Cambridge University Press, Cambridge, 1985).